17:11:39 OCA PAD INITIATION - PROJECT HEADER INFORMATION 03/31/89

Active

Project #: E-18-668 Cost share #: Rev #: 0
Center # : R6710-0A0 Center shr #: OCA file #:
Work type : RES
Contract#: N60921-89-M-2674 Mod #: Document : PO
Prime #: Contract entity: GTRC

Subprojects ? : N
Main project #:

Project unit: MAT ENG Unit code: 02.010.112
Project director(s):
SANDERS T H B JR MAT ENG (404)894-5793

Sponsor/division names: NAVY / NAVAL SURFACE WARFARE CTR, VA
Sponsor/division codes: 103 / 003

Award period: 890315 to 900314 (performance) 900401 (reports)

Sponsor amount	New this change	Total to date
Contract value	19,999.00	19,999.00
Funded	19,999.00	19,999.00
Cost sharing amount		0.00

Does subcontracting plan apply ?: N

Title: PROPOSED PROGRAM FOR ADDITIONAL TASK

PROJECT ADMINISTRATION DATA

OCA contact: E. Faith Gleason 894-4820

Sponsor technical contact

R.K. GARRETT
(202)394-2730
NAVAL SURFACE WARFARE CENTER
WHIT OAK
SILVER SPRING, MARYLAND 20903-5000

Sponsor issuing office

ANITA BURTON
(202)394-4982
NAVAL SURFACE WARFARE CENTER
WHITE OAK
SILVER SPRING, MARYLAND 20903-5000

Security class (U,C,S,TS) : U
Defense priority rating : DO-C9E
Equipment title vests with: Sponsor
NONE PROPOSED

ONR resident rep. is ACO (Y/N): N
supplemental sheet
GIT X

Administrative comments -
INITIATION. FIXED PRICE AWARD.

GEORGIA INSTITUTE OF TECHNOLOGY
OFFICE OF CONTRACT ADMINISTRATION

NOTICE OF PROJECT CLOSEOUT

Closeout Notice Date 02/12/91

Project No. E-18-668 Center No. R6710-0A0

Project Director SANDERS T H B JR School/Lab MAT ENGR

Sponsor NAVY/NAVAL SURFACE WARFARE CTR, VA

Contract/Grant No. N60921-89-M-2674 Contract Entity GTRC

Prime Contract No.

Title PROPOSED PROGRAM FOR ADDITIONAL TASK

Effective Completion Date 900314 (Performance) 900401 (Reports)

Closeout Actions Required:	Y/N	Date Submitted
Final Invoice or Copy of Final Invoice	Y	
Final Report of Inventions and/or Subcontracts	Y	
Government Property Inventory & Related Certificate	Y	
Classified Material Certificate	N	
Release and Assignment	Y	
Other	N	

Comments

Subproject Under Main Project No.

Continues Project No.

Distribution Required:

Project Director	Y
Administrative Network Representative	Y
GTRI Accounting/Grants and Contracts	Y
Procurement/Supply Services	Y
Research Property Managment	Y
Research Security Services	N
Reports Coordinator (OCA)	Y
GTRC	Y
Project File	Y
Other	N
	N

NOTE: Final Patent Questionnaire sent to PDPI.

CONTENTS

ILLUSTRATIONS

TABLES

CHAPTER 1

INTRODUCTION

Aluminum-Lithium alloys represent an appealing alternative to conventional high strength aluminum alloys for aerospace structural applications.[1] They possess a higher elastic modulus and lower density than the 2XXX and 7XXX alloys which have traditionally been used. In addition, Al-Li alloys can be heat-treated to high strength due to the precipitation of various metastable phases when magnesium and copper are also present in the alloy.

Zirconium is added to Al-Li alloys to form a fine dispersion of a metastable intermetallic phase, Al_3Zr. The small, coherent Al_3Zr particles are extremely effective at retarding subgrain boundary migration and coalescence, thus, inhibiting static recovery and recrystallization of hot-worked Al-Li alloys during post deformation heat treating operations.[2] While Zirconium in the form of the metastable Al_3Zr particles influences static recovery and recrystallization of aluminum alloys, the other solute elements such as magnesium in solid solution can have substantial effects on the dynamic processes occurring during hot working.

The limit of solid solubility for zirconium is 0.28 wt.%; however, from the point of view of casting an alloy containing zirconium, the composition at the break in the liquids curve (0.11 wt.% Zr) is the composition of interest. Compositions with zirconium contents in excess of this value run the risk of

containing the coarse primary Al-Zr phase. Alloys with up to approximately 0.18 wt.%Zr can be cast using small book-mold ingots where the solidification rate is relatively rapid. However, for large commercial ingots where the solidification rates are slow, the limits on the zirconium level must approach 0.11 wt.% or primary Al_3Zr will result.

In comparison with the precipitation-hardening elements such as lithium, magnesium and copper; zirconium has a relatively low diffusivity and tends to remain in solution after casting. Since the solute distribution coefficient k ($= C_s/C_l$) is slightly greater than unity, the zirconium tends to segregate in the interior of the dendrites rather than in the interdendritic channels where the eutectic elements such as lithium would be segregated. During the preheating cycle the lithium which is cored homogenizes and goes into solution, whereas the zirconium precipitates out of solution since the solid solubility of zirconium is small at the usual ingot preheating temperatures.

The zirconium precipitates from the supersaturated solution where it was located as a result of solidification coring. The result in a non-uniform distribution of Al_3Zr. Consequently, high strength ingot metallurgy alloys containing zirconium tend to have grain structures that are for the most part unrecrystallized but, because of the inhomogeneous distribution of Al_3Zr, regions of coarse recrystallized grains are often observed and the subgrain size distribution in the unrecrystallized portions of the microstructure tends to be broad. Thus, the non-uniform grain and

subgrain structures are at the TEM level of observation and at the optical level of observation. Although zirconium has a profound effect on the grain structure the major solute elements also play an important role in effecting the degree of recrystallization and substructure.

Alloys can respond to high temperature deformation by either dynamic recovery or dynamic recrystallization. Most research suggests that aluminum responds to hot deformation by dynamic recovery, a thermally activated event in which climb aided by cross-slip is the rate controlling mechanism.[3] During the recovery process, dislocation tangles form a cellular structure resulting in subgrains. However, when magnesium is added to aluminum, there is a corresponding reduction in the dynamic recovery capability of the alloy. This reduced recovery has been speculated to be caused by a reduction in the stacking fault energy of the alloy due to the magnesium in solid solution.[4] If sufficient magnesium is present in an alloy such that dynamic recovery is very difficult, dynamic recrystallization may occur. Dilute Al-Mg alloys containing 1 wt%* Mg,[5] 2% Mg,[6] and 3% Mg,[7] have shown dynamic recovery as the only softening mechanism, with subgrain sizes decreasing with increasing Mg concentration. However, studies with higher magnesium contents (5,7 and 10%) have shown evidence to support a dynamic recrystallization mechanism.[8]

* All compositions throughout the text will be given in weight percent.

In addition to compositional effects, recrystallization behavior and subgrain size are controlled by the processing variables under which the material is formed. The subgrain size which develops during high temperature metal working processes has been found to increase with increasing temperature for a given strain rate or with decreasing strain rate at a constant temperature.[9] Substantial property variations for a given alloy system can be observed between a recrystallized and unrecrystallized structure; strength, fracture toughness and fatigue behavior are all influenced by the degree of recrystallization in aluminum alloys.[10,11] Furthermore, corrosion resistance is affected by the degree of recrystallization.[12] Thus, the degree to which a given alloy recrystallizes is an important variable. Additionally, the size of the grains (recrystallized) or subgrains (unrecrystallized) has been found to have an effect on properties, particularly on strength in Al-Li alloys. In both cases, a finer structure leads to increased strength.[11,9] Grain (and subgrain) size can affect properties indirectly as well. Precipitation and coarsening behavior can be influenced by the presence of grain and subgrain boundaries, thereby further altering the final properties of the alloy.[13]

From the previous discussion, it is obvious that the deformation structure of an alloy is important in determining its final properties. In order to optimize material properties, both composition and processing variables must be considered. These variables control the microstructure and recrystallization behavior

of the alloy and, hence, contribute to its properties. In this report the effects that variations in composition and deformation temperature have on the substructure, and static recrystallization behavior of several Al-Li-Mg-Cu-Zr and Al-Li-Zr alloys are explored.

From the previous discussion a relationship between zirconium, deformation process and grain morphology occurs. An additional characteristic of an Al-Li-Zr alloy is the synergestic effect between lithium and zirconium. The presences of lithium tends to stimulate the precipitation of Al_3Zr. An important industrial consequence of the opposite reaction is also explored in this report.

During long term, high temperature soaks, lithium is lost at the surface. With this lithium loss there is a corresponding development of a recrystallized lager. An addition thurst of this research is to examine the recrystallization behavior of an Al-Li-Zr alloy and relate the development of the recrystallization lager to lithium loss.

In addition to retarding recrystallization, the Al_3Zr particles affect the nucleation, growth and coarsening of the Al_3Li (δ') particles in lithium-containing aluminum alloys. The similarities between δ' and β' permit the nucleation of β' directly on the pre-existing β' particles, resulting in a bimodal distribution of δ' particles. The average particle size of the composite δ' particles (δ' on β') is larger than the β'-free δ' particles. Furthermore, a comparison of the coarsening rate

constants for the two different types of δ' particles shows that the rate constant for the coarsening of the composite δ' particles is significantly greater than for the β'-free δ' particles. Because of the small volume fraction of β' the number of composite particles is less than the number of β'-free δ' particles; however, comparisons of BF and DF micrographs of the same area always show a thin shell of δ' around each β' particle. Since the β' phase appears to facilitate the nucleation of δ', an appropriate choice of quenching and aging practices could lead to a method to rapidly determine the thermodynamic solvus boundary of the δ' phase.

Consequently, an additional thrust of this research is to establish a rapid method of determining the δ' solvus boundary, to extend the composition region over which the boundary is known, to establish a boundary below which a uniform distribution of δ' would occur, and to demonstrate the feasibility of using this technique in complex Al-Li-Cu-Mg-Zr alloys.

CHAPTER 2

EXPERIMENTAL PROCEDURES

Seven of the most commercially promising Al-Li alloys were chosen for this study. These alloys, their nominal compositions, and their letter designations (A-G) are listed in Table 2-1.

TABLE 2-1. NOMINAL ALLOY COMPOSITIONS (WT%)

Designation	Alloy	Li	Cu	Mg	Zr
A	Navalite	2.0-2.1	0.9-1.5	3.0-3.1	0.12
B	Alcan	2.5	1.2	0.7	0.12
C	Lockalite	1.6-3.1	0.9-3.0	0.8-1.8	0.14
D	CP-276	1.9-2.6	2.5-3.3	0.2-0.8	0.04-0.16
E	CP-274	1.7-2.3	1.8-2.5	1.1-1.9	0.04-0.16
F	CP-271	2.2-2.8	1.1-1.7	0.7-1.3	0.08-0.16
G	2090	2.0	3.0	-	0.12

Three billets of each alloy, 15cm long, were individually cast by Mr. A.P. Divecha at the Naval Surface Warfare Center, White Oak, MD. Extrusion of these billets was carried out at R.M.I. Inc., Ashtibula, OH. The seven alloys were extruded at three different temperatures: 427°C, 399°C, and 343°C, designated 1,2, and 3, respectively. The 7.6 cm diameter billets were direct extruded through a lubricated conical die producing 3.8 cm x 0.64 cm (1½" x ¼:) rectangular sections -- an extrusion ratio of 19:1. Ram speed

for all extrusions was 1.9 mm/sec. The initial and final 20 percent of the product were discarded to insure that only the so-called steady-state region of the extrusion was being analyzed.

The Alcan alloy that was extruded at 399°C(B2) jammed on the run-out table during extrusion and was, therefore, not in an acceptable condition for evaluation in this study. The remaining 20 alloy/extrusion temperature combination products underwent spectrophotometric analysis for all elements except Lithium. Lithium and copper concentrations were determined by atomic absorption. All chemical analysis were made by Alcoa Technical Center.

Detailed metallographic examinations were made on the 20 extruded specimens. Microstructural features were examined using macroscopy, light optical microscopy, and transmission electron microscopy (TEM).

Macroscopic specimens were finely ground, macroetched in a concentrated NaOH solution for five minutes, and cleaned in a solution of concentrated nitric acid. Samples for light optical microscopy were mechanically polished lightly etched to reveal their grain structures. Electropolishing was performed in a solution containing 948 ml H_2O, 55ml HBF, and 7 gm H_3BO_3 for 45 seconds at 18 volts.

TEM observations were made on all 20 samples in the as-extruded and SHT conditions. TEM specimens were taken from the center of the extruded product at a 45° angle to the extrusion direction. Disks, 3mm in diameter, were electropolished using a

twin jet polisher, in a 3:1 methanol-nitric acid solution cooled by liquid nitrogen to approximately - 20°C. A JEOL-100 C operating at 100 kV was used for observation and photography of the foils. Quantitative analysis of the subgrain structure was necessary in order to find the average subgrain diameter, $\bar{d}$, of each sample. There are several methods by which this value can be determined. The following approach was chosen for this study. The number of subgrain boundary triple points, P, for a certain two-dimensional section, is directly related to the total number of subgrains, N_T, within that area by the relation:[14]

$$N_T = \frac{1}{2}P + 1 \qquad (2\text{-}1)$$

The number of subgrains per unit area, N_A, is by definition:[39,40]

$$N_A = N_T/AM \qquad (2\text{-}2)$$

where A is the physical area on which the measurement was taken, and M is the magnification. The number per unit area can be used to determine the average "diameter" of the cells within the structure by applying the ASTM definition of subgrain diameter:[15]

$$d = 1/\sqrt{N_A} \qquad (2\text{-}3)$$

A series of Al-Li-Zr alloys, Cu-Mg- as shown in Table 2-2 were chosen for cold working. Each alloy was chosen because the starting structure was unrecrystallized and the zirconium content varied across the series continuously from 0.06 to 0.12 wt% Zr. The alloys were solution heat treated (SHT) at 550°C, cold water quenched (CWQ), and examined by optical metallography, and TEM techniques. Optical metallographic surfaces

Table 2-2. ALLOY AND ZIRCONIUM CONTENT FOR COLD-WORK RECRYSTALLIZATION STUDIES.

Alloy Designation	wt% Zr
F3	0.06
F2	0.07
D2	0.08
D1	0.09
E1	0.10
F1	0.11
G1	0.12

were prepared as described above. TEM foils were prepared using the standard polishing techniques previously described.

Each of the hot worked slabs were cold rolled at 50% increments, SAT for 15 minutes CWQ, and again examined using optical metallography to estimate the degree of recrystallization then rolled another 50%. Consequently, the 1/2 slabes were rolled to 1/4", 1/8", 1/16" and 1/32" and examined for the degree of recrystallization.

Samples for a 1" extrusion of an Al-2.6 Li 0.09 Zr were hot rolled to 1/2". The samples were milled to insure parallel sides. Four samples were placed in an air furnace at 550°C for 2, 4, 8, and 12 hours. After the heat treatment at 2, 4, and 8 hours, there

was neglible oxide formation and the final dimension of the heat treated samples were close to those before heat treatment. However, at 12 hours of the heat treatment temperature, sevxxx oxidation of the surfaces was observed. The dept of the recrystallized layer was determined from optical samples taken after the different anneals.

Eight samples were placed in a salt batch at 550°C for 12, 24, 50, 60, 70, 80, 100 and 150 hours. The depth of the recrystallized layer was determined on each sample.

To establish the δ' thermodynamic solvus boundary, alloys were SHT at 550°C in a molten salt bath, CWQ, and aged at a variety of temperatures in the vicinity of the expected solvus boundary from the literature[16]. The aging times and temperatures were adjusted such that for the more concentrated alloys and higher aging temperatures, shorter aging times (on the order of minutes) were used to suppress the formation of a large volume fraction of anodic, coarse equilibrium δ (AlLi). There was also an attempt to examine TEM samples which would exhibit approximately the same amount of coarsening: for every 10°C drop in temperature, the aging time was doubled. Furthermore, by examining a range of temperatures below the δ' solvus boundary the influence of undercooling on the uniformity of δ' in unrecrystallized and recrystallized microstructures could be determined.

CHAPTER 3

RESULTS AND DISCUSSION

3.1 MATERIAL CHARACTERIZATION

The results of the spectrophotometric composition analysis performed by Alcoa are shown in Table 3-1. Since each billet was individually cast, significant composition variations were present for each of the three billets of a specific alloy type. The zirconium levels showed the largest variation of all the compositional variables. Atomic absorption was used to determine the Li and Cu concentrations of each alloy are and also summarized in Table 3-1.

3.2 CALCULATION OF THE TEMPERATURE COMPENSATED STRAIN RATE, Z

The flow stress, σ, of a deforming metal or alloy frequently increases with increasing strain rate and decreasing temperature, obeying the following empirical equation:[9,17]

$$A\sinh(\alpha\sigma)^n = Z = \epsilon\exp(+Q_{def}/RT) \qquad (3\text{-}1)$$

where A, α, n, and Q_{def} are constants, R is the gas constant, T is absolute temperature, ϵ is the strain rate and Z is the Zener-Holloman parameter, also known as the temperature compensated strain rate.

The subgrain size of hot worked aluminum is found to be uniquely related to Z by equations of the form:[9,18,19]

$$d^{-1} = a + b\ln Z \qquad (3\text{-}3)$$

Therefore, calculation of the Zener-Holloman parameter as a

TABLE 3-1. COMPOSITIONS OF THE ALLOYS

Alloy ID	Alloy/Extr. Temp.	Li	Cu	Mg	Zr
A1	Navalite/427°C	2.27	1.58	3.47	0.04
A2	Navalite/399°C	2.25	0.92	3.16	0.10
A3	Navalite/343°C	2.50	1.14	3.05	0.06
B1	Alcan/427°C	2.25	2.41	1.19	0.02
B2	-	-	-	-	-
B3	Alcan/343°C	2.09	1.52	1.16	0.11
C1	Lockalite/427°C	2.49	1.16	0.84	0.11
C2	Lockalite/399°C	3.53	1.16	0.82	0.09
C3	Lockalite/343°C	3.35	1.28	0.85	0.06
D1	CP-276/427°C	2.04	2.92	0.64	0.09
D2	CP-276/399°C	2.07	2.83	0.58	0.08
D3	CP-276/343°C	2.30	2.58	0.56	0.03
E1	CP-274/427°C	1.77	2.16	1.48	0.10
E2	CP-274/399°C	1.81	2.26	1.62	0.04
E3	CP-274/343°C	1.97	2.20	1.58	0.09
F1	CP-271/427°C	2.29	1.32	1.08	0.11
F2	CP-271/399°C	2.54	1.26	1.06	0.07
F3	CP-271/343°C	1.67	1.74	1.12	0.06
G1	2090/427°C	1.85	2.85	-	0.12
G2	2090/399°C	2.11	2.99	-	0.11
G3	2090/343°C	1.96	3.12	-	0.11

(Fe + Si) < 0.12

function of processing variables is an essential step in relating processing to substructure. In order to estimate Z, the values Q_{def}, ϵ, and T must be determined. Determining these parameters often requires significant assumptions and approximations to be used. The method of determining the three parameters needed to

calculate Z will be discussed below.

Determination of Q_{def}

In the formalism of equation (3-1), Q_{def} is considered as an activation energy for deformation and is approximately equal to the activation energy for self-diffusion in high stacking fault energy metals.[20] This value is equal to ~ 155 kJ/mole for aluminum.[9,17] It is a function of composition; however, Castle and Sheppard[21] noted that Q_{def} ranged from 156 to 164 kJ/mole for a large range of compositions and suggested that a value of 160kJ/mole was a reasonable approximation of the activation energy for the alloys under observation. Since the formalism requires Q_{def} to be constant for a given composition over the range in hot-working temperatures,[22] this value of Q_{def} was applied under all three extrusion temperatures.

Determination of the Mean Equivalent Strain Rate, $\dot{\bar{\epsilon}}$

In order to calculate the strain rate by which to characterize a material, it must be understood that the strain and strain rate during extrusion are neither constant nor independent of position.[21] Extrusion B2, which jammed in the run-out, was only partially extruded. Therefore, it was possible to section the remaining billet and macroetch the surface in order to observe the material flow pattern which developed during extrusion. A heterogeneous strain distribution across the section was observed. Despite this heterogeneous strain distribution, it is necessary to calculate a mean equivalent strain rate, $\dot{\epsilon}$, in order to relate the processing variables to the microstructure and properties of the product.

The most common approach used to calculate this value was developed by Feltham[23], who suggested a time averaged method that is based on the equation:

$$\dot{\bar{\epsilon}} = \frac{\textit{total strain, } \epsilon}{\textit{time taken to produce that strain, } t}$$

The total strain can be written as

$$\epsilon = \ln R \tag{3-4}$$

where R is the extrusion ratio (A_o/A_f). The time required to produce the total strain can be expressed as

$$t = \frac{\text{volume of the die}}{\text{volume of metal extruded per unit time}} \tag{3-5}$$

For a die having a semiconical angle, α and a large extrusion ratio, the time required to cause the total strain, for a given volume of material can be approximated by:

$$t = \frac{D}{6V \tan\alpha} \tag{3-6}$$

where V is the ram speed, and D is the billet diameter. This leads to an approximate mean equivalent strain rate given by:[24]

$$\dot{\bar{\epsilon}} = \frac{\epsilon}{t} = \frac{6V(\ln R)\tan\alpha}{D} \tag{3-7}$$

Since the product in this study was not circular, the notion of a semiconical angle, α is not valid. However, the actual die angles did not differ significantly from 45°, and the assumption of a cone

of 45° leads to a die volume of approximately that estimated by measurements of the actual die; thus, this value of α was chosen. In order to compensate for the non-circular extrusion product, the modified extrusion ratio, R', suggested by Sheppard and Wood was applied to equation (3-8):[25]

$$R' = R \quad P_e/P_r \tag{3-8}$$

where P_e is the extrusion perimeter, and P_r is the circumference of a rod having the same extrusion ratio. The empirically based correction factor was used to modify the temperature compensated strain rate, Z. Since strain rate was not varied in this study, any error in calculating ϵ will be consistent throughout, and this value is simply calculated to allow for comparison of Z with other published data.

Determination of the Mean Temperature, T

The temperature, the final quantity that needs to be known in order to calculate Z, was the independent variable that was modified in the experiment. Just as the mean equivalent strain rate was a somewhat ambiguous term to define, so is the mean temperature since the extrusion process is rarely isothermal. The actual temperature of extrusion is a function of several factors, which themselves are not constant during the process. The primary factors are as follows:[26]

1. Initial billet temperature
2. Heat generation due to plastic deformation, shear, and friction
3. Heat transfer within the billet
4. Heat transfer between the billet and the tooling,

5. Heat transferred with the extruded product upon exit.

Factor 4 generally acts to reduce the extrusion temperature below the initial billet reheat temperature, while 2 is the primary factor increasing it. Temperature rise during extrusion tends to dominate once extrusion commences, and an average temperature can be approximated using the integral profile technique[27] or others.[28,29] However, even when no attempt is made to account for temperature rise during processing, reasonable correlations between flow stress and Z have been observed.[30,31] Wong and Jonas[30] conducted such a study, calculating Z-based on the initial billet temperature. Additionally, correlations between Z (calculated from the initial temperature) and average subgrain diameter have been conducted with reasonable results.[32] In this work, the product exit temperature was not measured. Lacking sufficient data to make a more accurate estimate of the mean extrusion temperature, the approach used by Wong and Jonas[55], and Parson and Sheppard[32] was employed, and the initial billet temperature was used to calculate Z.

3.3 VARIATION OF THE AS-EXTRUDED STRUCTURE WITH COMPOSITION AND TEMPERATURE COMPENSATED STRAIN RATE, Z

All of the extruded products showed a dynamically recovered structure consisting of subgrains appearing slightly elongated when observed with TEM in the longitudinal direction. This directionality decreased with decreasing extrusion temperature such that the subgrain structures of the samples extruded at the lowest temperature were nearly equiaxed. Internal dislocation densities tended to be slightly higher for the high Z extrusions, and

stringer particles were observed in all of the alloys at each extrusion temperature. Quantitative microscopy was performed on each of the alloys. Subgrains appeared nearly equiaxed when viewed from the 45° angle chosen for the analysis. Consistent studies by workers[9,19,20] on other aluminum alloy systems, the substructure for a given alloy was found to be finer with decreased extrusion temperature. Table 3-2 summarizes the subgrain size data for each of the alloy/extrusion-temperature combinations.

TABLE 3-2. AVERAGE SUBGRAIN "DIAMETERS" (μm) AS-EXTRUDED

	Extrusion Temperature		
ID	1	2	3
A	2.38	2.20	1.69
B	2.87	-	1.74
C	2.78	2.29	1.79
D	2.72	2.36	2.01
E	2.64	2.47	1.97
F	2.49	2.23	1.88
G	2.30	2.09	1.74

Subgrain size has been shown in many alloy systems to be related to Z by the relation[31]

$$d^{-m} = a + b\ln Z \qquad (3\text{-}9)$$

where a, b, and m are constants. Most researchers have agreed that the value of m = 1 provides the best correlation for aluminum and its alloys:[9,18,19]

$$d^{-1} = a + b\ln Z \qquad (3\text{-}10)$$

Thus, equation (3-10) would be expected to hold true for the alloys under investigation. According to Sellars,[9] the values of a and b are nearly constant for a given base material, varying little with solute content. However, the relative subgrain sizes for pure aluminum versus Al-5%Mg for a given Z have been reported as approaching 1.6.[33] Due to the strong effect that substructural changes can have on mechanical properties, small changes in subgrain sizes can be viewed as significant, and the effect of composition should not be ignored.

The variation in subgrain size with temperature compensated strain rate is shown for each of the alloys in Figure 3-1. A least squares fit based on equation (3-11) was applied in order to determine the coefficients a and b for each alloy. The results of this correlation are shown in Table 3-3. The constants a and b for each alloy should be applied with caution for several reasons. The alloys studied had significant composition differences at the three values of Z, due to the individual casting of the extrusion billets. Further, only three points were used (two points for alloy B) to make the correlation, and only a relatively small range of Z was studied. Also, equation (3-10) relating subgrain size and temperature compensated strain rate is subject to substantial experimental scatter. For example, work reported on Al-Li-Mg alloys by Parson and Sheppard[32] showed variations in subgrain size at a given Z for a single alloy on the order of the variation observed between the seven alloys in this study at a given Z.

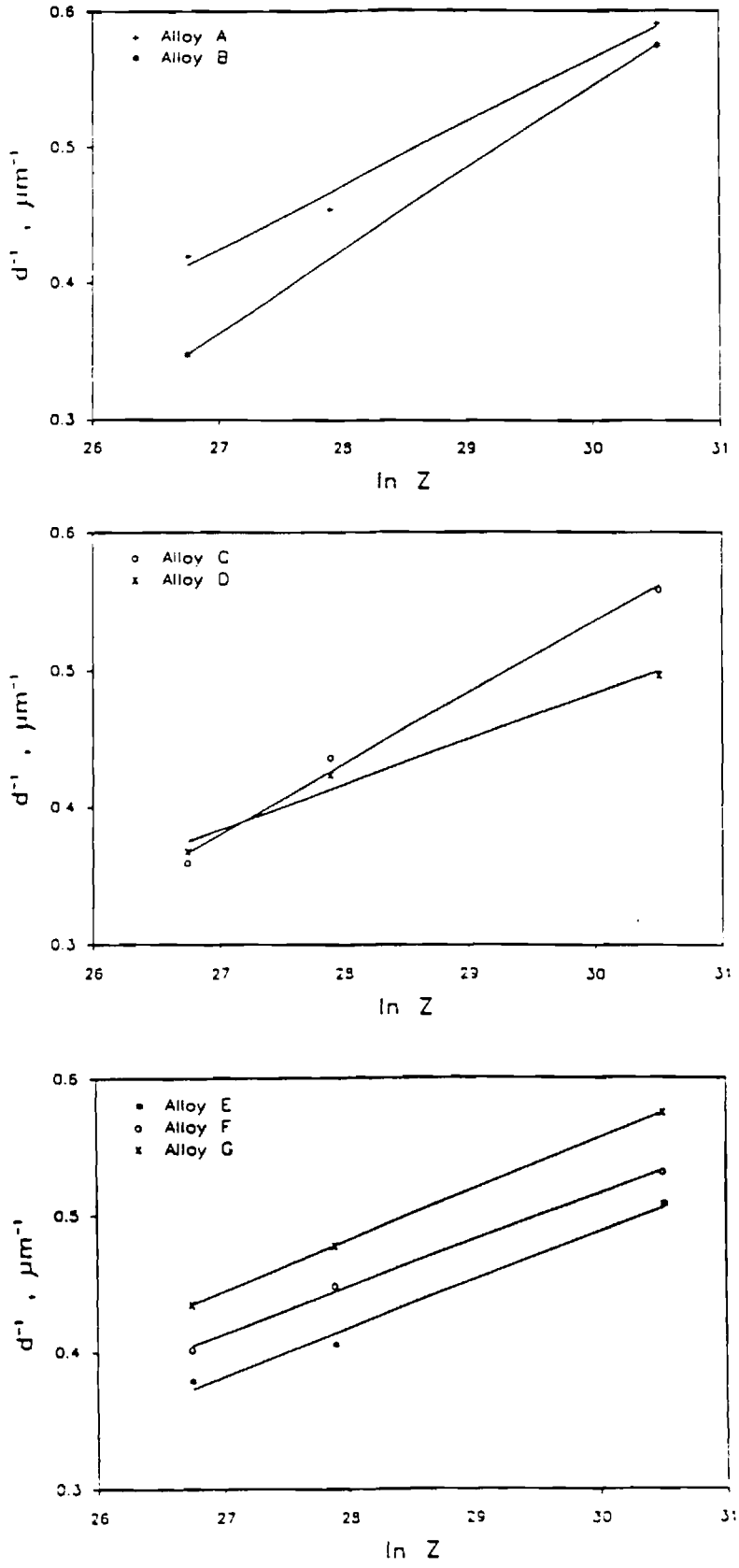

FIGURE 3-1 VARIATION IN SUBGRAIN SIZE, d, WITH TEMPERATURE COMPENSATED STRAIN RATE, Z, FOR EACH ALLOY

Due to the significant composition variations of the alloys relative to their nominal values, coupled with limited experimental data, the effect of composition on the size of the as-extruded substructure which forms during the processing of the Al-Li-Mg-Cu-Zr alloys can not be firmly established by this study. However, the correlation that as-extruded subgrain size increased with increased extrusion temperature (decreased Z) holds true for the Al-Li-Mg-Cu-Zr system as seen in Figure 3-2.

TABLE 3-3. COEFFICIENTS a AND b FROM $d^{-1} = a + b \ln Z$

	a	b
A	-0.85	0.047
B	-1.27	0.061
C	-1.02	0.052
D	-0.52	0.033
E	-0.57	0.035
F	-0.51	0.034
G	-0.56	0.037

3.4 VARIATION OF THE SHT STRUCTURE WITH COMPOSITION AND TEMPERATURE COMPENSATED STRAIN RATE, Z

The SHT substructures were observed using TEM. A partially retained substructure was observed in all but four alloy/extrusion temperature combinations; A1, B1, E2, and D3. TEM studies were unable to detect any substructure in these four specimens, suggesting that static recrystallization had occurred during the

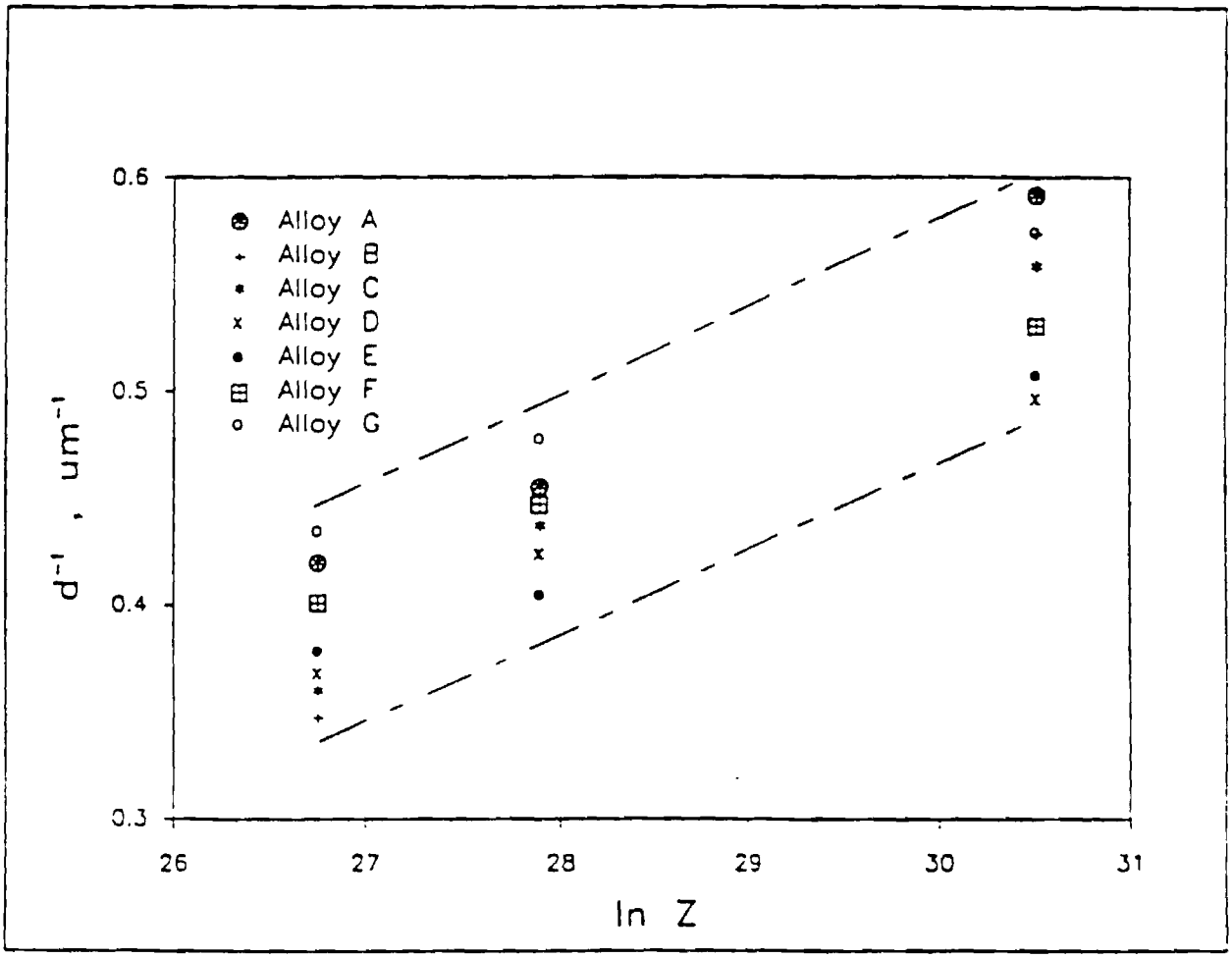

FIGURE 3-2. TREND OF SUBGRAIN SIZE VARIATION WITH Z FOR THE Al-Li-Mg-Cu-Zr SYSTEM

solution heat treatment. Optical microscopy confirmed that static recrystallization had taken place in each of these alloys; fully recrystallized grains were present in each case.

A detailed TEM analysis was performed on the other 16 specimens. Dislocation densities were lower, subgrain walls were more clearly defined, and the subgrain size was substantially larger than in the as-extruded condition, indicating that static recovery had occurred during the solution soak. The stringer particles observed in the as-extruded specimens were no longer present, suggesting that a sufficient heat treatment temperature and time had been chosen. Quantitative TEM was undertaken to determine the SHT subgrain size of each alloy. The results of this study are listed in Table 3-5. The functional relationship between d and extrusion temperature that was observed for the as-extruded alloys did not hold true for each of the alloys in the SHT condition. For example, alloy C3 had a larger substructure than did C2. Any attemt to correlate subgrain size and Z for particularly since four of the samples contained no substructure. Thus to correlate each of these alloys with equation (3-10) would be futile. The size of the subgrain structure retained through the solution soak was found to be a function of the zirconium content of that alloy as well as Z. Table 3-5 lists the Zr concentration of the alloys. By comparing Tables 3-4 and 3-5, it can be seen that, in general, greater than expected subgrain growth in some of the low extrusion temperature samples (e.g. C3) is directly

TABLE 3-4. AVERAGE SUBGRAIN "DIAMETERS" AFTER SOLUTION HEAT TREATING

	EXTRUSION TEMPERATURE		
ID	1	2	3
A	*	3.43	3.03
B	*	-	2.46
C	3.94	2.67	2.77
D	3.55	2.68	*
E	3.63	*	2.78
F	3.18	2.65	2.49
G	3.35	2.82	2.38

* No substructure observed

correlated with low zirconium content in the alloys. The zirconium, precipitated out nonuniformly as a fine dispersion of metastable Al_3Zr, is known to be an effective inhibitor to subgrain boundary motion.[2]

High Zr alloys, such as G3, underwent significantly less subgrain growth during SHT than did alloys low in zirconium. The higher volume fraction of Al_3Zr particles and smaller interparticle spacings seen in the high Zr alloys resulted in a greater retarding force to subgrain growth. Alloy 2090, G, was the only alloy exhibiting no significant Zr content variation under the three extrusion temperatures. Since G1, G2, and G3 each contained high Zr concentrations, the SHT substructure showed a similar relation

TABLE 3-6. Zr CONCENTRATIONS IN THE DIFFERENT ALLOYS

	Extrusion Temperature		
ID	1	2	3
A	0.04	0.10	0.06
B	0.02	-	0.11
C	0.11	0.09	0.06
D	0.09	0.08	0.03
E	0.10	0.04	0.09
F	0.11	0.07	0.06
G	0.12	0.11	0.11

to extrusion temperature as did the as-extruded alloys.

The increased subgrain size with increasing extrusion temperature (decreasing Z) can clearly be seen. Substantial recovery had occurred during the SHT cycle and, thus, a much larger subgrain size than that of the as-extruded alloy was observed. Since zirconium contents were nearly equal in this alloy, there is reason to believe that the recovery of the substructure was controlled to a similar degree for each extrusion temperature during the solution soak. Thus, a similar relationship between the average subgrain size and Z as was found for the as-extruded alloys could be present for this alloy in the solution heat treated condition. Figure 3-3 shows the d^{-1} versus Z relation for the SHT

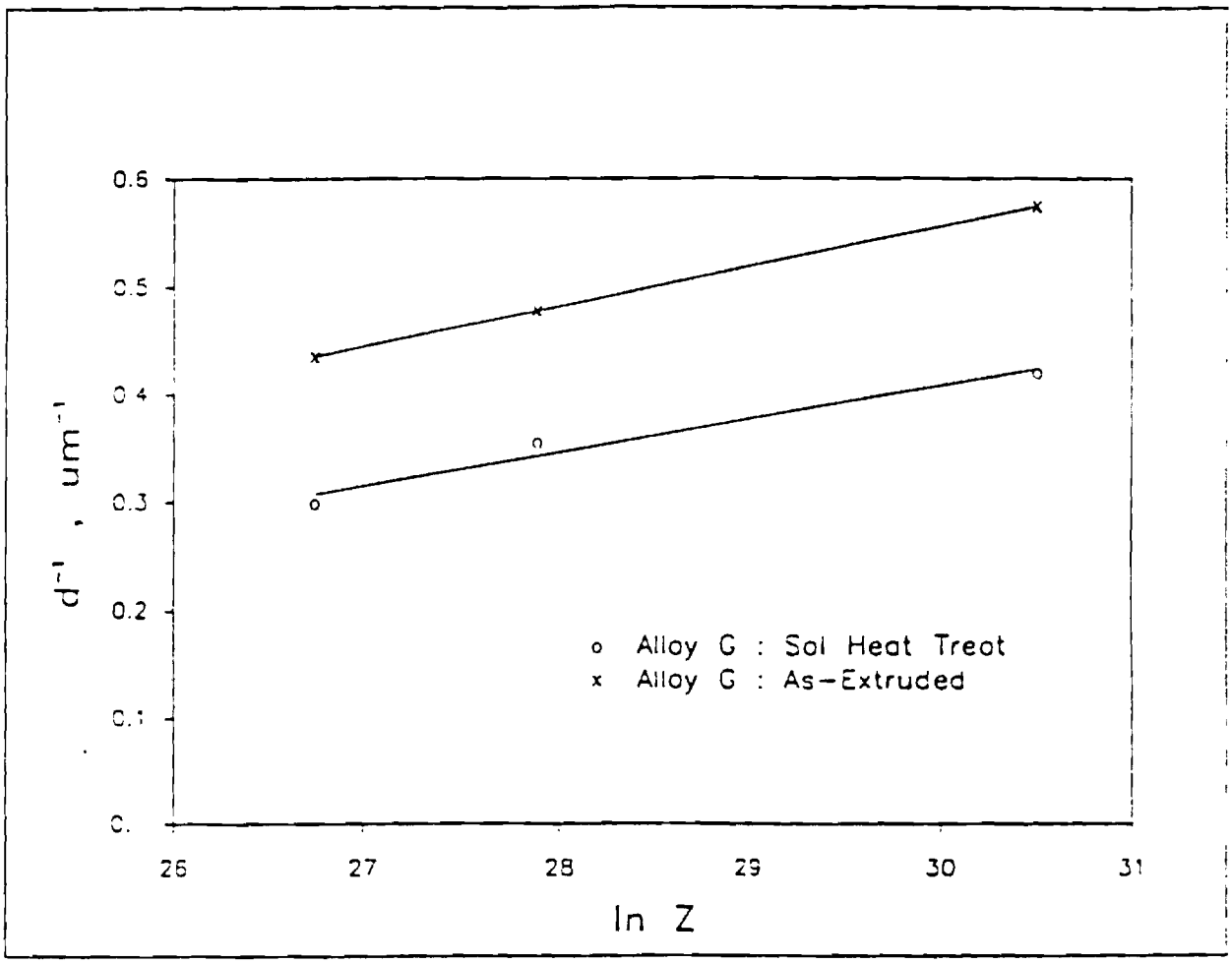

FIGURE 3-3. VARIATION IN SUBGRAIN SIZE, d, WITH TEMPERATURE COMPENSATED STRAIN RATE, Z, IN THE AS-EXTRUDED AND SHT CONDITIONS FOR ALLOY 2090 (G)

condition together with the as-extruded data on the alloy for comparison. A correlation based on equation (11) yielded the expression:

$$d^{-1} = -0.52 + 0.031(\ln Z) \qquad (3\text{-}12)$$

The values of a and b are quite similar to those of the alloy in the as-extruded condition. The significant separation between the lines in indicative of the static recovery that occurred during SHT which resulted in substantial subgrain growth.

3.5 EFFECTS OF COMPOSITION AND EXTRUSION TEMPERATURE ON STATIC RECRYSTALLIZATION

3.5.1 Influence of Zirconium

The complete static recrystallization observed in some of the alloy/extrusion temperature combinations can also be explained by the zirconium content variations of the alloys. The four samples which fully recrystallized during the SHT all had zirconium concentrations of 0.04 percent.

The samples which did not fully recrystallize had 0.06 percent $\leq$Zr$\leq$0.12 percent, suggesting that a minimum Zr concentration is needed to prevent complete recrystallization. Since fully recrystallized structures occurred under each of the extrusion conditions (A1 and B1, E2, D3), it appears that the minimum zirconium concentration needed to prevent complete recrystallization is relatively independent of the extrusion parameters. Further, Mg and Cu compositions do not have a substantial influence on the required zirconium content necessary to avoid recrystallization. At a given extrusion temperature,

complete recrystallization occurred (A1, B1) and was prevented (C1, D1, E1, F1, G1) for similar zirconium concentrations, despite large variations in Mg and Cu concentrations.

The zirconium concentration not only determined which alloys would fully recrystallize after not working and a post deformation anneal, but it was the primary factor in controlling the degree to which each alloy recrystallized. For a given extrusion temperature, the degree of recrystallization that the alloys underwent during SHT increased with decreasing Zr content. The degree to which the alloys statically recrystallized at 520°C ranged from almost completely unrecrystallized in the high (0.11%) Zr alloys to totally recrystallized in the low (0.03%) Zr alloy, with Mg and Cu concentrations playing a relatively insignificant role by comparison. In a subsequent section (3.6) the influence of Zirconium level on cold-work material will be described.

3.5.2 Influence of Extrusion Temperature

In order to determine the effect of extrusion temperature on static recrystallization, alloy 2090, G, was chosen for analysis. Only this alloy had a relatively constant zirconium content at the three extrusion temperatures so that the variations in recrystallization seen at the different extrusion temperatures could be attributed to temperature effects rather than compositional variations of Zr. Alloys G1, G2, G3 were SHT at 540°C. The structures were observed by optical microscopy. Each alloy exhibited a mixed structure consisting of original elongated

grains in addition to fine statically recrystallized grains. These recrystallized grains tended to be present primarily at the original grain boundaries, consistent with the fact that high stresses are present at these boundaries due to localized misfit, hence, promoting the nucleation of recrystallization.[32] The degree of recrystallization and the size of the recrystallized grains proved to be a function of extrusion temperature with decreased extrusion temperature increasing both of these parameters substantially. Figure 3-3 illustrates this relationship through a comparison of the degree of recrystallization for ally G as a function of extrusion temperature. It should be noted that slightly less recrystallization was observed in alloy G3 when it was SHT at 520°C.

3.6 RECRYSTALLIZATION OF COLD-WORK Al-Li-Zr-Y Alloys

The results of the metallographic examinations showed a correlation between the zirconium content and the tendency to recrystallize after cold roling and are summarized as follows:

1. 0.06% Zr is necessary to maintain a partially unrecrystallized microstructure after hot working in the range of 340-430°C and annealing at temperatures above 550°F.

2. The resistance to recrystallization progressively increases with increasing Zr content for microstructures cold worked after hot working.

3. Zirconium contents on the order of 0.11% Zr prevents recrystallization even after significant cold rolling. It should be pointed out however, the recrystallization anneals were less than 0.25 hours and even the most resistant alloy may recrystallize if annealed for longer times.

4. A detailed summary related to amount fo deformation and degree of recrystallization is given in Table 3-6.

TABLE 3-6 AMOUNT OF RECRYSTALLIZATION FOR ALLOYS, AS A FUNCTION FINAL ROLLED THICKNESS, IN PERCENTAGES

Alloy	wt.% Zr				
F3	.06	80	100	100	100
F2	.07	20	100	100	100
D2	.08	10	90	100	100
D1	.09	10	80	100	100
E1	.10	<10	70	100	100
F1	.11	<10	30	40	100
G1	.12	0	0	0	0

The recrystallization behavior in the Al-Li system is important for two reasons:

1. maintenance of strength, and
2. provide a microstructure with the best combination of strength and ductility

3.7 THE INFLUENCE OF LITHIUM LOSS ON SURFACE RECRYSTALLIZATION

Alloys containing lithium readily oxidize during high temperature heat treatment. A number of reactions are possible depending upon temperature, alloy, and atmosphere in contact with the alloy. Wefers and Mozelewski[36] have analyzed possible chemical reactions and those summarized in Table 3-7 are the reactions which over the temperature range for normal heat treating have $G<0$. Although there are other possible reactions that are thermodynamically permissible those reported in Table 3-7 represent the reaction products most frequently encountered on heat treated products[37].

TABLE 3-7 THERMODYNAMICALLY ADMISSABLE REACTIONS WITH PRODUCTS MOST OFTEN ENCOUNTERED DURING HEAT TREATING

$4Li + O_2 -> 2Li_2O$
$2.5Li + 0.5Al + H_2O -> 0.5LiAlO_2 + 2LiH$
$2Li + H_2O -> Li2O + H_2$
$Li_2O + CO_2 -> Li_2CO_3$

Unlike conventional non-Li containing aluminum alloys the oxidation products found on Al-Li alloys are permeable to lithium and when heat treated in air, the phase Li_2CO_3 appears as a brittle, loosely adherent coating which is often cracked. Consequently, Li can continuously diffuse from the alloy through the cracked surface coatings resulting in lithium loss which continues to grow through the heat treatment cycle. The growth of the Li-depleted region follows the form: [52]

$$x = \sqrt{mt} + c$$

where m and c are constants depending upon composition and temperature. This relationship has been shown to apply to 8090, 2090, 2091[38] and to 01420, the Soviet Al-Mg-Li alloy[39].

With the loss in Li there is a concomitant growth of the recrystallization layer at the surface[37]. The loss in Li reduces the effectiveness of the zirconium as a recrystallization inhibitor and consequently a recrystallization layer develops and continuously increases with increasing time at temperature. The depth of the recrystallized layer is plotted in Figure 3-4 for the

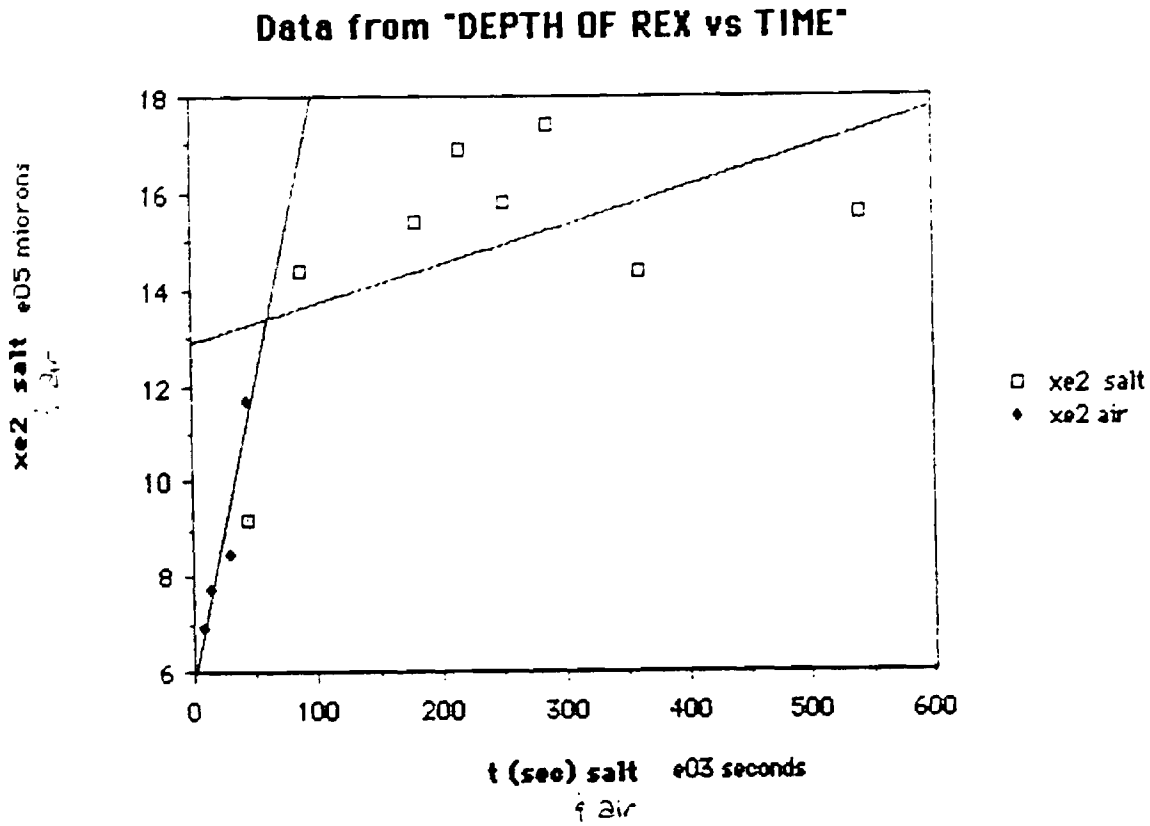

FIGURE 3-4 THE INFLUENCE OF TIME AT TEMPERATURE ON THE DEPTH OF THE RECRYSTALLIZED LAYER IN Al-2.6Li-1.09Zr ALLOY.

Al-Li-Zr alloy heat treatet in air and in salt. The alloy heat heated in air continues to recrystallize at longer times following the initial slope, whereas when heat treated in salt the dept of the recrystallized region levels and remains relatively constant. Consequently, when exposed for long soak times at elevated temperatures lithium loss leads to a recrystallized layer which continues to grow with time.

3.8 DETERMINATION OF THE $\delta'(Al_3Li)$ SOLVUS BOUNDARY

Solvus determination for the Al-Li-Zr alloys made in this investigation, along with the data of Baumann and Williams, are plotted in Figure 3-5. Assuming the relation ln X vs. 1/T is linear, a least-squares analysis was used to calculate the solvus. The experimental data points are included in the plot. This solvus boundary was determined as the aging temperatures above which no Al_3Li formed. Figure 3-6 shows a micrograph taken from a sample aged at 295°C, presenting an example of precipitates found in this sample. Only composite particles with a thin shell of Al_3Li are observed. Figure 3-7, taken from a sample aged at 300°C, shows few particles, with uniform intensity throughout the β', and a thin envelope surrounding each, rather than the donut contrast of the composite particles. The background shows a dispersion of very fine δ' particles. The same type of fine δ' distribution has been observed in solution heat treated, and water-quenched binary alloys[34] and in the background of ternary Al-Li-Zr alloys which have been solution treated, quenched, and aged above the solvus temperatures[35]. This latter treatment also shows the same particles

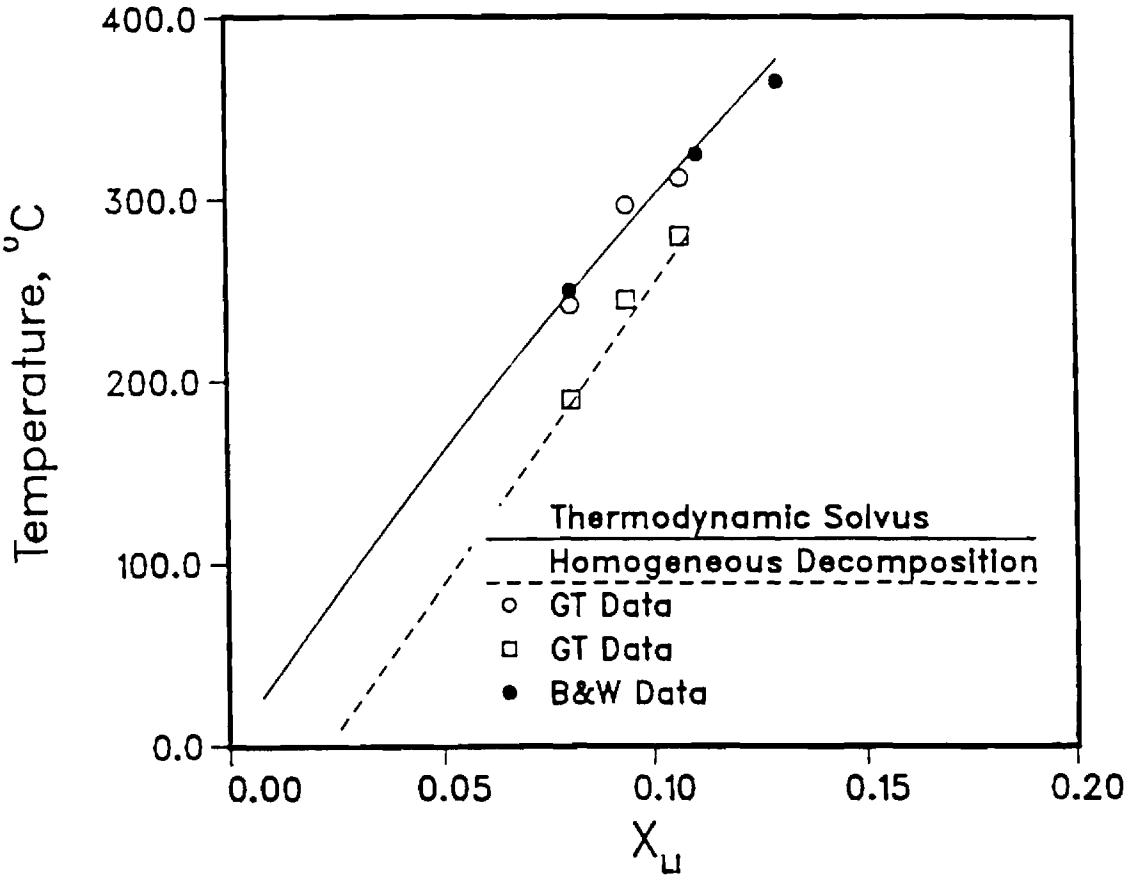

FIGURE 3-5 PORTION OF THE Al-Li PHASE DIAGRAM SHOWING EXPERIMENTAL (THIS WORK AND LITERATURE[16]) AND CALCULATED SOLVUS AND HOMOGENEOUS DECOMPOSITION BOUNDARIES

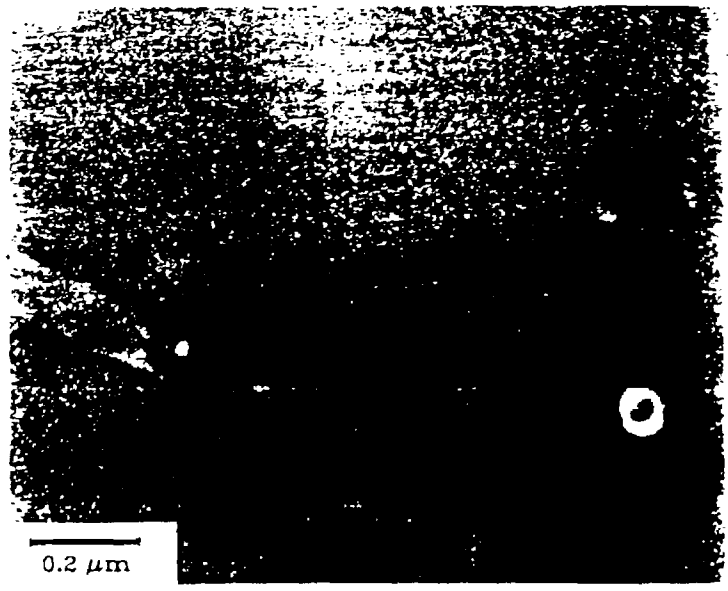

FIGURE 3-6 DF IMAGE OF COMPOSITE PARTICLE IN Al-Li-Zr SAMPLE AGED AT 295°C.

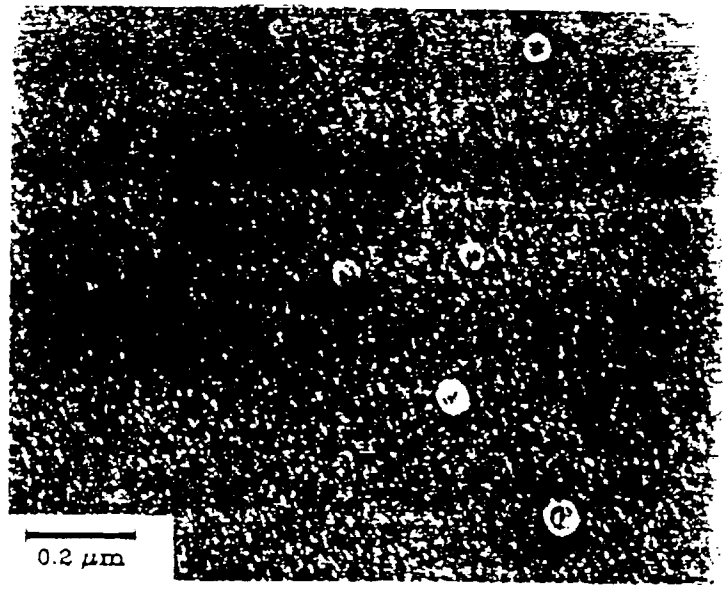

FIGURE 3-7 DF IMAGE OF COMPOSITE PARTICLES IN SAMPLE, BUT AGED AT 300°C.

with the thin envelope of δ'. The finely dispersed particles are δ' formed during the quench to room temperature, either from the solution heat treating temperature, or from the aging temperature. Clearly, since little or no δ' has formed upon aging at the highest temperature in our study, this is above the solvus for this composition. Similar investigations were performed for other zirconium-containing aluminum-lithium alloys, with 2.2 and 3.0 wt.% Li, and these data were also used to generate the solvus plotted in Figure 3-5.

For the Al-2.6Li-.09Zr alloy, the change in appearance of the distribution of precipitates from homogeneous to heterogeneous arises during the change in aging temperature from 240° to 250°C, which indicates the boundary for homogeneous decomposition occurs at about 245°C. An example of the determination of this boundary is illustrated with Figures 3-8 and 3-9, TEM DF images of samples aged at 240° and 260°C, respectively. Figures 3-8a and 3-8b show the homogeneous distribution at a subgrain boundary and in the bulk of a recrystallized grain, the former exhibiting a precipitate free zone (PFZ) but no particles at that boundary which have undergone coarsening. The onset of inhomogeneous precipitation at the higher temperature is shown in Figures 3-9a and 3-9b, with distributions at similar subgrain boundary sites. By halving the temperature intervals to within 5°C, this boundary was determined for this composition as 245°C. Similar investigations on the 2.2 and 3.0 wt. % Li alloys result in the second, lower line in Figure 3, the homogeneous boundary for Al_3Li precipitation in Al-Li-Zr alloys.

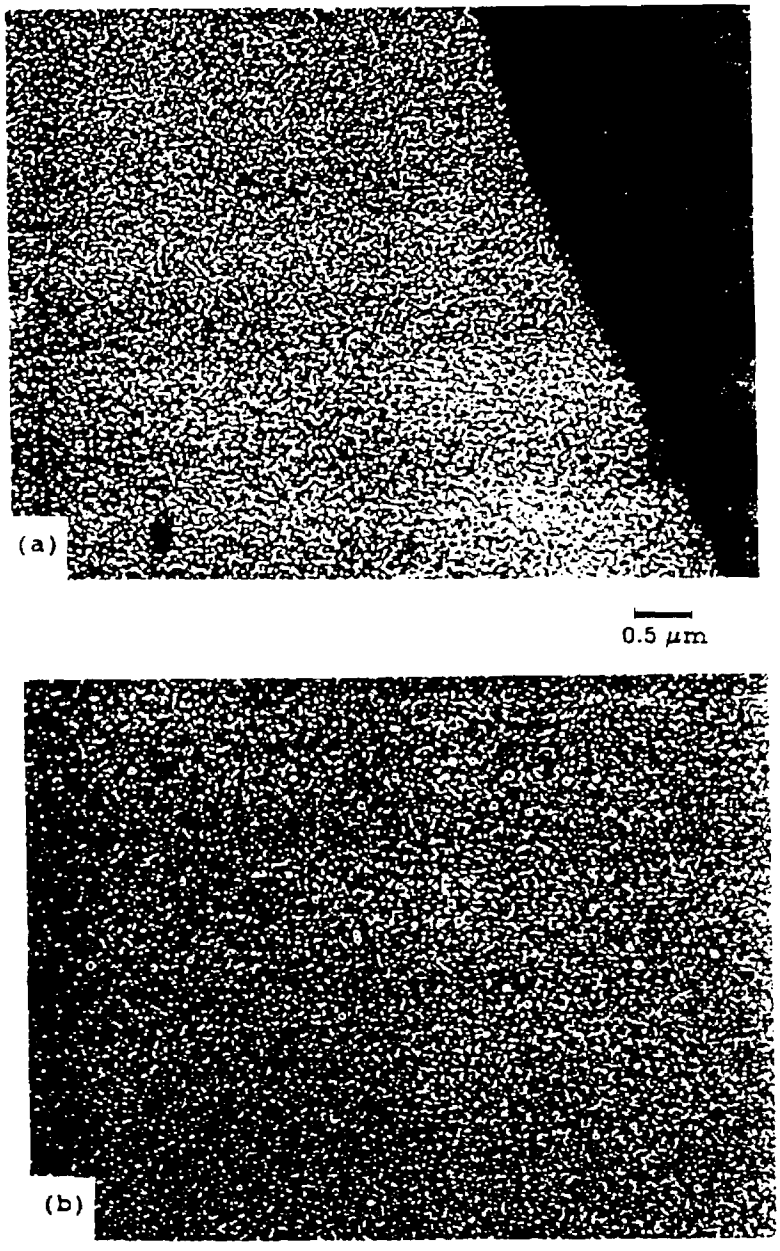

FIGURE 3-8 DF MICROGRAPHS OF Al-Li-Zr SAMPLE AGED AT 240°C, SHOWING PRECIPITATE DISTRIBUTION (a) AT SUBGRAIN BOUNDARY AND (b) IN BULK OF GRAIN.

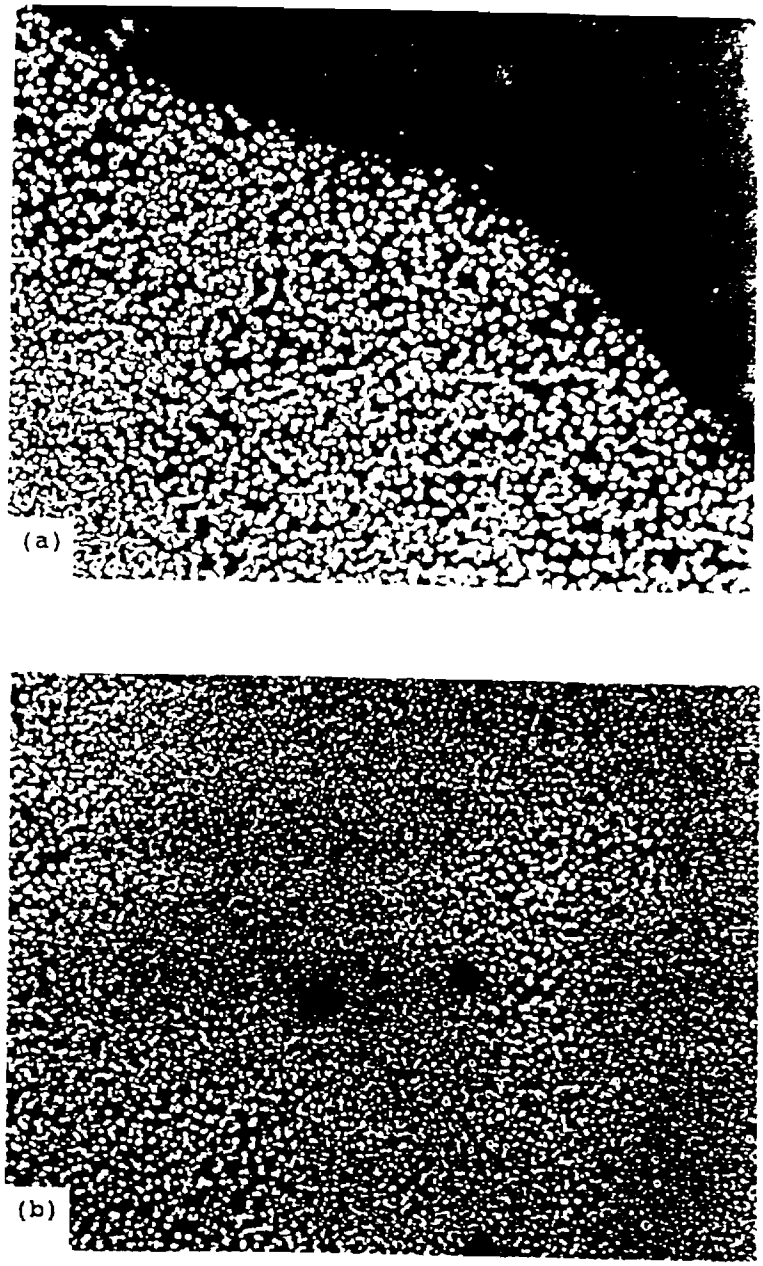

FIGURE 3-9 SAME ALLOY AS FIGURE 3-8, BUT AGED AT 260°C.

These inhomogeneities were observed by Baumann and Williams[34], and the temperatures below which the homogeneous decomposition occurs, about 40 or 50°C below the δ' solvus, agrees well with their findings.

Another important observation was made and should be pointed out. Figure 3-10 contains a BF and DF pair showing the presence of an unrecrystallized microstructure. Two types of subgrain boundary heterogeneous nucleation are observed. On one boundary a high density of closely spaced δ' is observed. No noticeable PFZ is present, however. On another boundary, a δ' PFZ was observed, along with the heterogeneous nucleation and growth of the equilibrium δ phase. It is anticipated that this variation in the type of precipitate nucelated, and the corresponding width of the PFZ is related to boundary misorientation. δ' nucleation primarily restricted to special boundaries. One would also anticipate that this variation in PFZ width would have an effect on ductility and would also occur in other more complex Al-Li-X alloys. This will be considered during the next quarterly report period focusing on the alloys summarized in Table 1.

Alloy	Experimental δ' Solvus	Expected δ' Solvus	Solvus Shift	Homog. Decomp.
N1	250°C	236°C	+14°C	215°C
N2	247°C	236°C	+14°C	212°C
N3	252°C	233°C	+19°C	215°C
N4	250°C	237°C	+13°C	217°C
N5	247°C	237°C	+10°C	215°C

As can be seen in Table 3-7, changes are observed in both the solvus and the homogeneous decomposition boundaries with addition

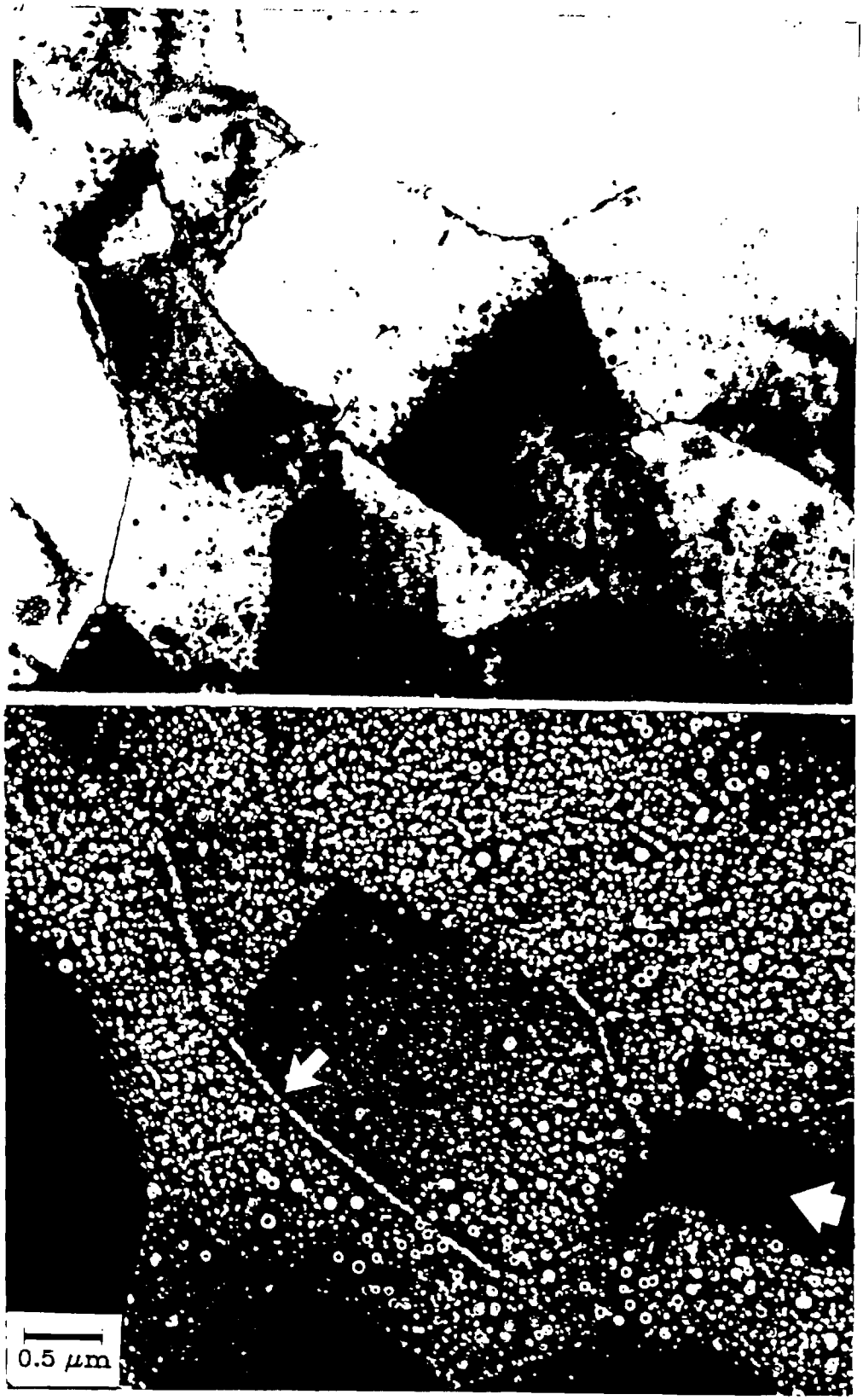

FIGURE 3-10 (a) BF AND (b) DF SHOWING NON-UNIFORM PRECIPITATE FREE ZONES AT DIFFERENT SUBGRAIN BOUNDARIES ADJACENT TO ONE ANOTHER.

of further components to the alloys, again making use of the distributions observed in TEM micrographs. The change in copper concentration does not seem to have a marked effect on the solvus temperature, confirming the behavior of the solvus observed by Baumann and Williams[16]. In that same work, a decrease in solubility of Li was observed in the alloy due to a presence of Mg, raising the solvus temperature of δ'. Accepting the negligible effect of Cu on the solubility, the change in solubility of Li in our alloys agrees with the previous observation of the effect of Mg. The solvus temperature of 250°C is higher than that expected for a binary alloy of the same Li content, about 233°C. The homogeneous precipitation boundary for this composition of Li is about 215°C.

The use of the δ'-on-β' heterogeneous precipitation phenomenon obviates the concern for including capillarity effects in the determination of the solvus boundary. The β' particles facilitate the nucleation of the Al_3Li, so while a distinct amount of undercooking is necessary to precipitate the δ' homogeneously, an aging temperature below the solvus is not required to form the shell of δ' on the β' spheres. Indeed, the results described above indicates a range of temperature of about 5 to 10°C in which no β' - free δ' particles have formed, only the composite particles. This temperature range in which homogeneous nucleation will not occur compares favorably with the value obtained by Baumann and Williams in their attempt to establish a coherent solvus.

CHAPTER 4

SUMMARY

1. The as-extruded substructure which forms in these alloys is a strong function of extrusion temperature. The average subgrain diameter can be related to the temperature compensated strain rate, Z, through the equation, $d^{-1} = a + b\ln Z$.
2. Alloys containing 0.04 percent Zr statically recrystallized during solution heat treating, regardless of Mg and Cu concentrations or extrusion temperature.
3. In alloys containing 0.06 percent Zr 0.12 percent, subgrain growth and static recrystallization were observed during the SHT. The degree or recrystallization tended to be a much stronger function of the Zr content than of the Mg and Cu concentrations or the temperature at which the metal forming process occurred.
4. For alloy 2090, which contained equal concentrations of Zr at each extrusion temperature, the degree of static recrystallization during SHT was found to increase with decreasing extrusion temperature.
5. Solution heat treated samples that were not fully recrystallized showed a substructure in the unrecrystallized regions that was a function of Zr concentration as well as Z. The equation, $d^{-1} = a + b\ln Z$, was valid only for the alloy having equal Zr content for all three extrusion conditions.

6. A minimum Zirconium content of 0.06 wt. percent was necessary to suppress the recrystallization of a solution heat heated hot worked product.
7. Increasing the zirconium content beyond 0.06 wt. percent progressively increases the resistance to recrystallization as measured by introducing cold work by rolling.
8. Surface recrystallization is associated with lithium loss due to oxidation. When heat treating is conducted in an inert salt bath surface recrystallization is minimized. When heat treating is conducted in an air furnace, surface recrystallization and oxidation are catostrophic.
9. The precipitation of δ' on pre-existing β' particles appears to be an effective method of establishing the δ' solvus boundary.

CHAPTER 5

REFERENCES

1. Sanders, Jr. T.H. and Stark, Jr. E.A. "Aluminum-Lithium Alloys II", conference proceedings TMS-AIME, T.H. Sanders, Jr. and E.A. Stark, Jr., eds., 1984, pp. 1-16.

2. Starke, Jr. E.A., Sanders, Jr., T.H. and Palmer, I.G. J. of Metals, 33, 1981, pp. 24-33.

3. Jonas, J.J., Sellars, C.M. and McG. Tegart, W.J. Metall. Rev., 14, 1969 pp. 1-24.

4. Truszkowski, W., Pawlowski, A. and Dutrewicz, J. Bull. Acad. Pol. Sci., 19, 1971, p.55.

5. McQueen, H.J. and Conrod, K. Microstructural Control in Aluminum Alloys: Deformation, Recovery, and Recrystallization, The Metallurgical Society, Inc. E.H. Chia and H.J. McQueen, eds., 1986, pp. 197-219.

6. Zaidi, M.A., Title Ph.D. Thesis University of London Imperial College, 1980.

7. Tutcher, M.G., Title Ph.D. Thesis, University of London Imperial College, 1979.

8. Sheppard, T., Zaidi, M.A., Tutcher, M.G. and Parson, N.C. Microstructural Control in Aluminum Alloys: Deformation, Recovery, and Recrystallization, The Metallurgical Society, Inc., E.H. Chia and H.J. McQueen, eds., 1986, pp. 155-178.

9. Sellars, C.M. Aluminium Transformation Technology and Applications, 1978, pp. 405-440.

10. Sanders, Jr., T.H. Final Report-Naval Air Development Center, Contract No. N62269-76-C-0271, June 1979.

11. McElroy, R.J. and Szkopiak, Z.C. International Met. Reviews, 17, 1972, pp. 175-202.

12. Niskanen, P., Sanders, Jr., T.H., Marek, M. and Rinker, J.G.: Aluminum-Lithium Alloys, conference proceedings TMS-AIME, T.H. Sanders, Jr., and E. A. Starke, Jr., eds., 1981, pp. 347-376.

13. Niskanen, P., Sanders, Jr., T.H., Rinker, J.G. and Marek, M. Corrosion Science, 22, 1982, pp. 283-304.

14. E.E. Underwood: Quantitative Stereology, Addison-Wesley, Mass., 1970, pp. 10-11.

15. ASTM E112-63, Standard Methods for Estimating the Average Grain Size of Metals.

16. S.F. Baumann and D.B. Williams, Aluminum - Lithium Alloys II, ed. E.A. Starke, Jr. and T.H. Sanders, Jr., TMS-AIME, Warrendale, PA (1984) pp. 17-29.

17. H.J. McQueen and J.J. Jonas: J. Appl. Metal Working, 4, 1984, pp.233-241.

18. H.J. McQueen and J.J. Jonas: Treatise on Material Science and Tech., 6, Academic Press, New York, 1975, p. 404.

19. H.J. McQueen and J.J. Jonas: Plastic Deformation of Materials, R.J. Arsenault, ed., Academic Press, New York.

20. T. Sheppard: Metals Technology, April 1981, pp. 130-141.

21. A.F. Castle and T. Sheppard: Metals Technology, Oct. 1976, pp. 454-463.

22. D. Raybould and T. Sheppard: J. Inst. Metals, 1973, pp. 65-73.

23. P. Feltham: Metal Treat and Drop Forging, 23, 1956, pp. 440-444.

24. G.E. Dieter: Mechanical Metallurgy, McGraw-Hill, Inc., 1976, p. 652.

25. T. Sheppard and E.P. Wood: Metals Technology, Feb. 1980, pp. 58-66.

26. K. Laue, and H. Stenger: Extrusion, American Society for Metals, Ohio, 1981.

27. T. Sheppard and D. Raybould: J. Inst. Metals, 89, 1960, p. 225.

28. M.M. Farag and C.M. Sellars: J. Inst. Metals, 101, 1973, pp. 137-145.

29. J.J. Jonas and T. Chandra: Metal Forming: Interrelation between Theory and Practice, A.L. Hoffmanner, ed., Plenum Press, New York, 1971, p. 115.

30. W.A. Wong and J.J. Jonas: Trans. AIME, 242, 1968, p. 227.

31. T. Sheppard, M.A. Zaidi, P.A. Hollinshead and N. Raghunathan: Microstructural Control in Aluminum Alloys: Deformation, Recovery, and Recrystallization, The Metallurgical Society, Inc., E.H. Chia and H.J. McQueen, eds., 1986, pp. 19-43.

32. N.C. Parson and T. Sheppard: Aluminum-Lithium Alloys II, conf. proc. TMS-AIME, T.H. Sanders, Jr. and E.A. Starke, Jr., eds., 1984, pp. 53-64.

33. J.R. Cotner and W.J. McG. Tegart: J. Inst. Metals, 97, 1969, pp. 73-792.

34. S.F. Baumann and D.B. Williams, Acta Metall, 33 (1985) pp. 1069-1078.

35. F.W. Gayle and J. B. Vander Sande, Acta Metall., 37 (1989) pp. 1033-1046.

36. Wefers, K. and Mozelewski, F.A., Proc. 8th International Light Metals Conference, Vienna, Australia, (1987), pp. 744-750.

37. Partridge, P.G., "A Review of the Oxidation of Al-Li Alloys in the Solid and Liquid States," Technical Report 89037, Royal Aerospace Establishment, Farnborough, Hampshire (1989).

38. Holdway, P. and Bowen, A.W., Royal Aerospace Establishment Technical Report 88059, Farnborough, Hampshire (1988).

39. Fridlyander, I.N., Sandler, V.S., Nikdskya, T.I., Savinkow, R.A., and Roschina, I.N., Russian Met. 2, (1978), p. 175.